

Orbital Surface Hopping from the Orbital Quantum-Classical Liouville Equation for Nonadiabatic Dynamics of Many-Electron Systems

Yong-Tao Ma,^{||} Rui-Hao Bi,^{||} and Wenjie Dou^{*}



Cite This: *J. Chem. Theory Comput.* 2025, 21, 3847–3856



Read Online

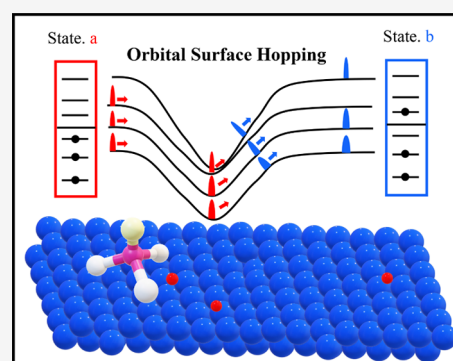
ACCESS |

Metrics & More

Article Recommendations

Supporting Information

ABSTRACT: Accurate simulation of the many-electron nonadiabatic dynamics process at metal surfaces remains a significant challenge. In this work, we present an orbital surface hopping (OSH) algorithm rigorously derived from the orbital quantum-classical Liouville equation (o-QCLE) to address nonadiabatic dynamics in many-electron systems. This OSH algorithm is closely connected to the popular independent electron surface hopping (IESH) method, which has demonstrated remarkable success in addressing these nonadiabatic phenomena, except that electrons hop between orbitals. We compare the OSH approach with the IESH method and benchmark these two algorithms against the surface hopping method using a full configuration interaction (FCI) wave function. Our approach shows strong agreement with IESH and FCI-SH results for molecular orbital populations and kinetic energy relaxation, while also exhibiting high efficiency, thereby demonstrating the capability of the new OSH method to capture key aspects of many-electron nonadiabatic dynamics.



1. INTRODUCTION

Nonadiabatic effects on metal surfaces, such as vibrational energy relaxation and electron transfer, play a crucial role in many physical and chemical processes, including inelastic collision^{1–5} chemisorption,^{6–8} electrochemistry,^{9,10} heterogeneous catalysis,^{11,12} and molecular junctions.^{13,14} Accurately describing these effects, particularly the interaction between nuclear motion and electronic degrees of freedom, presents a significant challenge due to the severe breakdown of the Born–Oppenheimer approximation. Moreover, the metal electronic orbitals form a continuum, facilitating surface electron–hole pair excitations. Consequently, treating these systems fully quantum mechanically would require considering an astronomical number of excited states. These factors make full quantum mechanical methods, such as multi configuration time-dependent hartree (MCTDH)¹⁵ and hierarchical quantum master equation (HQME),¹⁶ impractical for such systems.

For efficient simulations of more realistic metal interface systems, a mixed quantum-classical approach is necessary. Indeed, a variety of methods, such as electron friction theory (EF),^{17–26} independent electron surface hopping (IESH) method,^{27,28} Mapping Mode,²⁹ and broached classical master equation (BCME) methods,^{30,31} have recently been used to study the dynamics of metal surfaces. Among these methods, the EF and IESH methods are the most popular and widely used. Although EF theory is straightforward to implement and has seen significant development in recent years,^{32–43} it is inherently limited to the weak coupling regime. Specifically, its

applicability requires low nuclear momenta and weak nuclear–electron interactions. Furthermore, when analyzing vibrational energy dissipation, EF theory can accurately predict the average vibrational energy but fails to provide the correct vibrational state distribution.²⁸

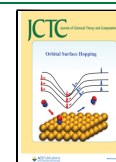
To address the limitations of the EF method, Tully’s group developed the IESH method in 2009.²⁷ The idea of IESH is very similar to the trajectory surface-hopping time-dependent Kohn–Sham (TDKS) approach proposed by Prezhdo and coworkers.^{44,45} A popular program called PYXAID, under this approach, focuses on nonadiabatic molecular dynamics in condensed matter systems and was developed accordingly.⁴⁶ While the IESH method was mainly applied to metal surfaces, e.g., the inelastic scattering between the NO molecule and the Au(111) surface, it successfully reproduces trapping probabilities and equilibrium vibrational energy distributions that align well with experimental results.⁴⁷ This demonstrates that IESH can capture key experimental trends with reasonable accuracy. Furthermore, it is computationally efficient due to the independent electron assumption, making it a highly practical and effective model. Since its development, IESH has

Received: December 26, 2024

Revised: March 7, 2025

Accepted: March 10, 2025

Published: March 21, 2025



been widely applied to open-shell species on metal surfaces.⁴⁸ Despite its successes, IESH remains an analog without rigorous proof. In this article, we demonstrate why the independent electron ansatz of IESH works by directly analyzing the many-body quantum dynamics of a noninteracting system. The main theoretical result is an orbital quantum classical Liouville equation (o-QCLE), which can naturally lead to an orbital surface hopping (OSH) algorithm. In addition, we perform full configuration space surface-hopping dynamics for small systems to demonstrate that both OSH and IESH capture the essential many-body dynamics despite being evolved with single-particle equations of motion.

This article is organized as follows. Section 2 comprises a comprehensive description of the methods and theory used in this paper, where Section 2.1 presents the derivation of the orbital quantum-classical Liouville equation. The o-QCLE can naturally lead to the OSH approach, which is presented in Section 2.2; in Section 2.3 we reconstruct the IESH method based on o-QCLE. Section 2.4 outlines the algorithm of full configuration interaction surface hopping (FCI-SH). Section 3 presents the numerical comparison of IESH, OSH, and FCI-SH over two systems, representing thermal equilibrium (Section 3.1) and high vibrational states (Section 3.2). Finally, we summarize this work in Section 4.

2. THEORY AND METHODOLOGY

2.1. The Orbital Quantum-Classical Liouville Equation. Consider a general many-electron Hamiltonian describing the coupled electron–nuclear motion, given by

$$\hat{H}_{\text{total}} = \hat{T}_n + \hat{H}_{\text{el}}(\mathbf{r}, \mathbf{R}) \quad (1)$$

where $\hat{T}_n \equiv \hat{\mathbf{P}} \mathbf{M}^{-1} \hat{\mathbf{P}}/2$ represents the nuclear kinetic operator, \hat{H}_{el} represents the electronic Hamiltonian that depends on electronic (\mathbf{r}) and nuclear (\mathbf{R}) coordinates. Suppose the electrons are noninteracting, such that \hat{H}_{el} can be described by quadratic terms

$$\hat{H}_{\text{el}}(\mathbf{r}, \mathbf{R}) = \sum_{ij}^m h_{ij}(\mathbf{R}) \hat{d}_i^\dagger \hat{d}_j + U(\mathbf{R}) \quad (2)$$

with \hat{d}_i^\dagger (\hat{d}_i) denoting the creation (annihilation) operator for the i (j)-th orbital, $h_{ij}(\mathbf{R})$ being the single-body Hamiltonian, and $U(\mathbf{R})$ representing the electronic state-independent potential energy. This system comprises m spin orbitals, which are occupied by n electrons distributed among these orbitals.

The many-body quantum dynamics of this molecular system is governed by the Liouville-von Neumann (LvN) equation, that

$$\frac{\partial \hat{\rho}}{\partial t} = -\frac{i}{\hbar} [\hat{H}_{\text{total}}, \hat{\rho}(t)] \quad (3)$$

where $\hat{\rho}(t)$ denotes the total many-body density operator. To proceed, we first define the single-body density operator $\hat{\sigma}$, whose matrix elements are given by $\hat{\sigma}_{kl} \equiv \text{Tr}_e(\hat{\rho} \hat{d}_l^\dagger \hat{d}_k)$. We can show that the single-body density operator satisfies (see detailed derivations in Appendix A)

$$\frac{\partial \hat{\sigma}}{\partial t} = -\frac{i}{\hbar} [\hat{H}_{\text{total}}^{\text{orb}}, \hat{\sigma}(t)] \quad (4)$$

Here $\hat{H}_{\text{total}}^{\text{orb}}$ represents the total Hamiltonian in the single-body basis set $\{|i\rangle, i = 1, \dots, m\}$:

$$\hat{H}_{\text{total}}^{\text{orb}} = \hat{T}_n + U(\hat{\mathbf{R}}) + \sum_{ij}^m h_{ij}(\mathbf{R}) |i\rangle \langle j| \quad (5)$$

again, $U(\mathbf{R})$ represents the pure nuclear potential energy. The single-body LvN eq 4 indicates that for a noninteracting many-electron system the dynamics are *exactly* encoded in the single-body Hamiltonian, as long as the system can be described by quadratic terms (eq 2).

We proceed by deriving a mixed quantum-classical Liouville equation for the orbital density matrix. To do so, we apply the partial Wigner transformation, which transfers the nuclear degrees of freedom from the Hilbert space to the phase space. For an arbitrary operator $\hat{O}(t)$, the Wigner transformation reads:

$$\hat{O}_W(\mathbf{R}, \mathbf{P}, t) = \int d\mathbf{Y} e^{-i\mathbf{P}\cdot\mathbf{Y}/\hbar} \left\langle \mathbf{R} - \frac{\mathbf{Y}}{2} \left| \hat{O}(t) \right| \mathbf{R} + \frac{\mathbf{Y}}{2} \right\rangle \quad (6)$$

and for the single-body density matrix $\hat{\sigma}$,

$$\hat{\sigma}_W(\mathbf{R}, \mathbf{P}, t) = (2\pi\hbar)^{-3N} \int d\mathbf{Y} e^{-i\mathbf{Y}\cdot\mathbf{P}/\hbar} \left\langle \mathbf{R} - \frac{\mathbf{Y}}{2} \left| \hat{\sigma}(t) \right| \mathbf{R} + \frac{\mathbf{Y}}{2} \right\rangle \quad (7)$$

where $3N$ is the size of the nuclear degrees of freedom. The trace of $\hat{\sigma}_W(\mathbf{R}, \mathbf{P}, t)$ over electronic degrees of freedom equals the number of electrons, m , as this is a many-electron system. By applying the partial Wigner transform rules to eq 4 and truncating the Wigner–Moyal operator to the first order,⁴⁹ we obtain the orbital quantum-classical Liouville equation (o-QCLE)

$$\begin{aligned} \frac{\partial \hat{\sigma}_W(\mathbf{R}, \mathbf{P}, t)}{\partial t} = & -\frac{i}{\hbar} [\hat{h}_W, \hat{\sigma}_W] - \sum_a \frac{P_a}{M_a} \frac{\partial \hat{\sigma}_W}{\partial R_a} \\ & + \frac{1}{2} \sum_a (\{\hat{h}_W, \hat{\sigma}_W\} - \{\hat{\sigma}_W, \hat{h}_W\}) \\ & + \sum_a \frac{\partial U}{\partial R_a} \frac{\partial \hat{\sigma}_W}{\partial P_a} \end{aligned} \quad (8)$$

Here, the Poisson bracket is

$$\{\hat{A}(\mathbf{R}, \mathbf{P}), \hat{B}(\mathbf{R}, \mathbf{P})\} = \frac{\partial \hat{A}}{\partial \mathbf{R}} \cdot \frac{\partial \hat{B}}{\partial \mathbf{P}} - \frac{\partial \hat{A}}{\partial \mathbf{P}} \cdot \frac{\partial \hat{B}}{\partial \mathbf{R}} \quad (9)$$

Finally, o-QCLE can be projected onto an adiabatic basis. We first diagonalize the single-body Hamiltonian to get the adiabatic orbital energy $\epsilon_j(\mathbf{R})$ and the corresponding basis $|\phi_j(\mathbf{R})\rangle$:

$$h(\mathbf{R}) |\phi_j(\mathbf{R})\rangle = \epsilon_j(\mathbf{R}) |\phi_j(\mathbf{R})\rangle. \quad (10)$$

Sandwiching both sides of eq 8 by $\langle \phi_j(\mathbf{R}) | \cdot | \phi_k(\mathbf{R}) \rangle$, we obtain

$$\begin{aligned} \frac{\partial \hat{\sigma}_W^{jk}(\mathbf{R}, \mathbf{P}, t)}{\partial t} = & -i\omega^{jk}\sigma_W^{jk}(\mathbf{R}, \mathbf{P}, t) \\ & + \sum_l \sum_a \frac{P_a}{M_a} (\sigma_W^{jl} d_{lk}^a - d_{jl}^a \sigma_W^{lk}) \\ & - \sum_a \frac{P_a}{M_a} \frac{\partial \sigma_W^{jk}}{\partial R_a} \\ & - \frac{1}{2} \sum_l \sum_a \left(F_a^{jl} \frac{\partial \sigma_W^{lk}}{\partial R_a} + \frac{\partial \sigma_W^{jl}}{\partial P_a} F_a^{lk} \right) \\ & + \sum_a \frac{\partial U}{\partial R_a} \frac{\partial \sigma_W^{jk}}{\partial P_a} \end{aligned} \quad (11)$$

where $\omega^{jk} = (\epsilon_j - \epsilon_k)/\hbar$. We have used the fact that

$$\langle \phi_j(\mathbf{R}) | \frac{\partial \hat{\sigma}_W(t)}{\partial \mathbf{R}} | \phi_k(\mathbf{R}) \rangle = \frac{\partial \sigma_W^{jk}(t)}{\partial \mathbf{R}} - \sum_l (\sigma_W^{jl} \mathbf{d}_{lk} - \mathbf{d}_{lk} \sigma_W^{lk}) \quad (12)$$

Here the nonadiabatic coupling matrix elements are given as

$$d_{jk}^a = \left\langle \phi_j(\mathbf{R}) \left| \frac{\partial}{\partial R_a} \right| \phi_k(\mathbf{R}) \right\rangle = -\frac{F_a^{jk}}{\hbar\omega^{jk}} \quad (13)$$

and the force can be calculated under the Hellmann–Feynman equation

$$F_a^{jk} = \langle \phi_j(\mathbf{R}) | [\partial h / \partial R_a] | \phi_k(\mathbf{R}) \rangle \quad (14)$$

2.2. Orbital Surface Hopping Method (OSH). With o-QCLE (eq 11), we propose an orbital surface hopping (OSH) algorithm. QCLE is the starting point of many mixed quantum-classical algorithms,^{50–52} and its connection with surface hopping has been thoroughly discussed in refs^{51,53,54}. Similarly, o-QCLE (eq 11) also implies a surface hopping algorithm, which is called OSH. Without considering decoherence,⁵¹ the OSH algorithm can be outlined step-by-step as follows.

1. We start by sampling the initial wavepacket with a swarm of trajectories. The initial position (\mathbf{R}), momentum (\mathbf{P}) and occupied orbitals are sampled according to the problem being investigated. In each trajectory, nuclear position (\mathbf{R}), nuclear momenta (\mathbf{P}), and adiabatic single-particle density matrix (σ) are propagated. In addition, an index array $\vec{\lambda} = \{\lambda_1, \dots, \lambda_n\}$ is used to track the occupation of n electrons in m adiabatic orbitals. Specifically, σ can be initialized by either occupying diabatic or adiabatic orbitals:

- Diabatic occupation. Initially, suppose n diabatic orbitals, $\xi = \{\xi_1, \dots, \xi_n\}$, are occupied. Then, the initial diabatic density matrix is given by

$$\sigma_{ij}^{\text{diabatic}} = \begin{cases} \delta_{ij} & i \in \vec{\xi} \\ 0 & i \notin \vec{\xi} \end{cases}$$

Adiabatic density σ can be obtained by $\sigma = U^\dagger \sigma^{\text{diabatic}} U$. The adiabatic index array $\vec{\lambda}$ is then stochastically sampled from adiabatic populations $\text{diag}(\sigma)$.

- Adiabatic occupation. For given adiabatic occupation configuration $\vec{\lambda}$, σ is given by

$$\sigma_{ij} = \begin{cases} \delta_{ij} & i \in \vec{\lambda} \\ 0 & i \notin \vec{\lambda} \end{cases}$$

Despite the initialization scheme, the initial density represent a mixed state whose trace is n .

2. Between time t and $t + \Delta t$, propagate \mathbf{R} , \mathbf{P} by the following equations of motion:

$$\dot{\mathbf{R}} = \frac{\mathbf{P}}{M} \quad (15)$$

$$\dot{\mathbf{P}} = -\frac{\partial U}{\partial \mathbf{R}} + \sum_{i=1}^n \mathbf{F}_{\lambda_i, \lambda_i} \quad (16)$$

Instead of being propagated on potential energy surface of the *active state*, the nuclei experience the single-particle forces of the occupied orbitals. σ is propagated with a smaller time step $\Delta t'$ under the equation of motion for single-particle density matrix,

$$\dot{\sigma}_{ij}(t) = -i\omega^{jk}\sigma_{ij}(t) - \frac{\mathbf{P}}{M} \cdot \sum_k (\mathbf{d}_{ik}\sigma_{kj} - \sigma_{ik}\mathbf{d}_{kj}) \quad (17)$$

3. At every smaller time step $\Delta t'$, we evaluate the hopping probabilities from each occupied orbital to the unoccupied orbitals. Using the fewest switches surface hopping (FSSH)⁵⁵ scheme, the hopping probability from occupied orbital λ_i to orbital j is,

$$g_{j \leftarrow \lambda_i} = \begin{cases} \max\{-2\text{Re}(\sigma_{j\lambda_i}^* \dot{\mathbf{R}} \cdot \mathbf{d}_{j\lambda_i}) \Delta t' / \sigma_{\lambda_i, \lambda_i}, 0\} & j \notin \vec{\lambda} \\ 0 & j \in \vec{\lambda} \end{cases} \quad (18)$$

The stochastic hopping algorithm is identical to that of FSSH,⁵⁵ albeit hopping will be considered for each occupied electron. To minimize hopping, no more than one electron is allowed to transition to a different orbital per nuclear propagating time step.

4. When a hop occurs between λ_i and j , the total energy must be conserved.^{51,54} Momenta are rescaled in the direction of the single-particle derivative coupling $\mathbf{d}_{j\lambda_i}$.⁵⁶

If the nuclei do not have enough kinetic energy, the hop is frustrated and this hopping attempt is ignored.

5. Return to step 2.

Similar to the original FSSH algorithm, physical quantities that are exclusively nuclear operators (e.g., position, momentum, kinetic energy, etc.) or electronic operators diagonal in the adiabatic representation (e.g., adiabatic orbital populations) can be directly computed via averaging over trajectories. Diabatic orbital populations, however, are evaluated with the density matrix approach:^{57,58}

$$P_a = \sum_{i=1}^n \left(|U_{a\lambda_i}|^2 + \sum_{j=1}^m \sum_{k=j}^m 2\text{Re}(U_{aj} \sigma_{jk} U_{ak}^*) \right) \quad (19)$$

Overall, we have presented an efficient surface hopping algorithm for noninteracting multiple electrons system. For the OSH method, we expect that the n -electron density matrix remains constrained to that of a single Slater determinant as well. This follows directly from the electronic equation of motion in eq 17. In the diabatic basis, eq 17 reduces to $\dot{\sigma} = -i[h, \sigma]$, which will remain constrained to that of a single Slater

determinant if the initial condition is a single determinant. This OSH algorithm completely considers orbitals and occupations rather than electronic states and hence will be very efficient for large systems. Readers familiar with the independent electron surface hopping (IESH) method will notice some similarity between OSH and IESH. We will compare these two methods in Section 2.3.

2.3. IESH Method. We can reconstruct the IESH method starting from o-QCLE. As derived in Section 2.1, the dynamics are exactly encoded in the single-body Liouville equation as long as the electronic interaction can be described by quadratic terms. Each electron in this system can evolve independently under the time-dependent Schrödinger equation or single-body density matrix, as shown in eq 17, which closely resembles our OSH approach.

Unlike OSH, electrons in the IESH hop between states. The density matrix elements used in the calculation of hopping probabilities are achieved by constructing the many-electron states' Slater determinant with occupied orbital wave functions.²⁷ If b_j^+ and b_j are the creation and annihilation operators for a particle in the adiabatic orbital basis $|\phi_j(\mathbf{R})\rangle$. Then the many-electron eigenstate can be obtained by populating the N_e of these one-electron orbitals in one Slater determinant.

$$|j\rangle = b_{j_{N_e}}^+, \dots, b_{j_2}^+ b_{j_1}^+ |0\rangle = |\phi_{j_1}, \phi_{j_2}, \dots, \phi_{j_{N_e}}\rangle \quad (20)$$

Analogy the definition of FSSH⁵⁵ hopping probability from state $|j\rangle$ to state $|l\rangle$ can be written as

$$g_{jl} = \max\left\{\frac{\Delta t B_{lj}}{A_{jj}}, 0\right\}, \quad (21)$$

in which,

$$B_{jl} = -2\text{Re}(A_{jl}^* \dot{\mathbf{R}} \cdot \langle j | \mathbf{d}(\mathbf{R}) | l \rangle) \quad (22)$$

The j_i and l_i are the electron occupied orbitals in states j and l respectively. The subscript i refers to the i^{th} electron. Here, we follow Tully's definition²⁷ using this structure to remove the antisymmetry of electrons. It is easy to verify (see detailed derivations in Appendix B) that the nonadiabatic coupling is zero unless only one pair of electron orbitals differs from each other, which means only single-electron hops need to be considered in the hopping rate calculation.

The density matrix elements A_{jl}^* and A_{jj} are calculated using the "general overlap method"⁵⁹

$$A_{jl} = \langle j | \Phi \rangle \langle \Phi | l \rangle \quad (23)$$

Here, the total wave function $|\Phi\rangle$ is a single Slater determinant state,

$$|\Phi\rangle = |\psi_1, \psi_2, \dots, \psi_{N_e}\rangle \quad (24)$$

Then, the many-electron inner product $\langle j | \Phi \rangle$ is given by the determinant value of the overlap matrix of the occupied orbitals:

$$\langle j | \Phi \rangle = |S|, \quad S_{ij} = \langle \phi_i | \psi_j \rangle \quad (25)$$

Generally, the computational cost of these determinants is proportional to N^3 . N is the dimension of the determinant. These will be the bottleneck of the IESH approach if we

calculate them directly.⁶⁰ A detailed discussion is given in Section 2.4.

2.4. Full Configuration Interaction Surface Hopping.

As discussed in Section 2.3, only one Slater determinant is used for the total many-electron wave function in the IESH method. To include the correlation energy of different electron occupations, we borrow the idea from electronic structure theory. The exact total many-electron wave function is defined as a linear combination of N_e electron trial function:⁶¹

$$|\Phi\rangle = c_0 |\Psi_0\rangle + \sum_{ar} c_a^r |\Psi_a^r\rangle + \sum_{\substack{a < b \\ r < s}} c_{ab}^{rs} |\Psi_{ab}^{rs}\rangle + \dots \quad (26)$$

where $|\Psi_0\rangle$ is the Hartree–Fock (HF)-like Slater determinant with the lowest energy orbitals occupied. $|\Psi_a^r\rangle$ are the Slater determinants involving single excitation, $|\Psi_{ab}^{rs}\rangle$ are the Slater determinants involving double excitation.

The time evolution of the electronic FCI density matrix is also governed by the quantum Liouville equation (eq 3). Upon applying the partial Wigner transformation and adopting the adiabatic representation $|\Phi_j(\mathbf{R})\rangle$, the resulting quantum-classical Liouville equation of the FCI density matrix takes the form:

$$\begin{aligned} \frac{\partial \hat{\rho}_w^{jk}(\mathbf{R}, \mathbf{P}, t)}{\partial t} = & -\frac{i}{\hbar} (E_j - E_k) \hat{\rho}_w^{jk} \\ & + \sum_l \frac{P}{M} (\rho_w^{jl} D_{lk} - D_{jl} \rho_w^{lk}) - \frac{P}{M} \frac{\partial \rho_w^{jk}}{\partial \mathbf{R}} \\ & - \frac{1}{2} \sum_l \left(E_w^{jl} \frac{\partial \rho_w^{lk}}{\partial \mathbf{P}} + \frac{\partial \rho_w^{jl}}{\partial \mathbf{P}} E_w^{lk} \right) \end{aligned} \quad (27)$$

Starting from this QCLE, we can derive the FCI-SH algorithm step-by-step, as outlined in Section 2.2. For instance, a sort of electron can evolve according to the many-body Schrödinger equation.

$$i\hbar |\dot{\Psi}_i\rangle = H_{\text{el}}(\mathbf{R}(t)) |\Psi_i\rangle \quad (28)$$

It is worth noting that the hop probability from surface j to surface l , g_{jl} is also defined as

$$g_{jl} = \max\left\{\frac{\Delta t B_{lj}}{A_{jj}}, 0\right\} \quad (29)$$

and,

$$\begin{aligned} B_{jl} = & -2\text{Re}(A_{jl}^* \dot{\mathbf{R}} \cdot \langle \Psi_j | \mathbf{d}(\mathbf{R}) | \Psi_l \rangle) \\ = & -2\text{Re}(A_{jl}^* \dot{\mathbf{R}} \cdot \langle j | \mathbf{d}(\mathbf{R}) | l \rangle) \end{aligned} \quad (30)$$

This is identical to the hopping probability equation in the IESH approach, suggesting that the IESH method accounts for all electron excitations. A comparison of the dynamic results between IESH and FCI-SH will clearly demonstrate the impact of the many-body wave function on the dynamic process.

Finally, to use information on unoccupied states as mentioned in Section 2.2, the population of the diabatic state is calculated using the correct density matrix (CMD) method^{58,62} as eq 19. For evolution processes of IESH and FCI-SH are similar to the OSH approach. The details are provided in Section 2.2, so we will not repeat here.

3. RESULTS AND DISCUSSIONS

In this work, we focus on two questions: (1) Have any many-body effects been missed in the nonadiabatic dynamic simulation when using single-particle approaches such as OSH and IESH? (2) Can the new, simpler OSH approach achieve comparable or even better results than IESH? To address these questions, we study two nonelastic collision processes between a molecule and a metal surface. One scenario involves the molecule being under thermal equilibrium before collision, which is a simplified model used to study the electron transfer rate in chemisorption. The other scenario involves the molecule being highly vibrationally excited, which can demonstrate the state-to-state energy transfer mechanism in the fast electron transfer process.

For both systems, we employ the Newns–Anderson model, which has been successfully applied to study nonadiabatic effects at gas-metal interfaces.^{27,47} Numerous reference results using IESH are also available.^{58,63,64} For smaller systems, we use the FCI-SH approach as a many-body benchmark. For larger systems, comparisons are limited to OSH and IESH.

The Newns–Anderson Hamiltonian with one molecular orbital and a continuum of metal electron orbitals is given as

$$\hat{H}_{\text{el}}(\mathbf{R}) = U_0(\mathbf{R}) + (U_1(\mathbf{R}) - U_0(\mathbf{R}))c_a^\dagger c_a + \int_{E_-}^{E_+} d\epsilon (\epsilon c_c^\dagger c_c) + \int_{E_-}^{E_+} d\epsilon (V(\epsilon; \mathbf{R})c_a^\dagger c_c + V(\epsilon; \mathbf{R})^* c_c^\dagger c_a) \quad (31)$$

where $U_0(\mathbf{R})$, $U_1(\mathbf{R})$ are the potential energy surfaces of the neutral and anionic molecule, respectively. $V(\epsilon; \mathbf{R})$ represents the couplings between molecular and metal orbitals. $c_c^\dagger(c_c)$ and $c_a^\dagger(c_a)$ are the Fermionic creation and annihilation operators of metal and molecular orbitals, respectively.

To explicitly simulate this model, we discretized the integrals in eq 31. Specifically, the wide-band spectral density function is used, and the hybridization function,

$$\Gamma(\epsilon; \mathbf{R}) \equiv 2\pi \sum_k |V(\epsilon, \mathbf{R})|^2 \delta(\epsilon - \epsilon_k) \quad (32)$$

is assumed to be a constant Γ across the interval $E_- = -W/2 + \mu$ and $E_+ = W/2 + \mu$. Here, W and μ are the bandwidth and chemical potential, respectively. The trapezoid discretization procedure is adopted following ref 64, as it is reported to be numerically more stable⁶⁴ and equally accurate as the Gauss–Legendre procedure for small bandwidths.⁶⁰ For n_b metal orbitals, the discretized energies (ϵ_k) and the couplings (V_{ak}) are given as

$$\epsilon_k = \mu - \frac{W}{2} + W \frac{k-1}{n_b-1}$$

$$V_{ak} = \sqrt{\frac{\Gamma}{2\pi\rho}} \quad (33)$$

where $k = 1, \dots, n_b$ and the one-electron state density $\rho = n_b/W$.

For the potential energy surfaces, we consider a 1D double-well potential following refs^{58,60,63,64}

$$U_0(R) = \frac{1}{2}M\omega^2 R^2 \quad (34)$$

and linear orbital energy,

$$U_1(R) - U_0(R) = -M\omega^2 gR + \frac{1}{2}M\omega^2 g^2 + \Delta G \quad (35)$$

Here, the displacement parameter g is related to the reorganization energy by $E_r = \frac{1}{2}M\omega^2 g^2$.

Throughout Section 3, the occupation of the metal orbitals is prepared at "zero temperature," i.e., all the diabatic orbitals below the Fermi level μ are occupied. The impurity molecular orbital, on the other hand, remains unoccupied. Section 3.1 presents the thermal equilibrium results; hence, the trajectories are initialized at thermal equilibrium in the U_0 well. In this case, additional nuclear friction $\gamma_{\text{ext}} = 2\omega$ is applied to all trajectories to account for phononic energy dissipation on the surface.⁶⁴ Section 3.2 presents the vibrational relaxation results, where the trajectories are initialized at a high vibrational state ($\nu = 16$) using Wigner distribution sampling⁶⁵ of the U_0 harmonic potential. Finally, the parameters used in Section 3.1 and Section 3.2 are summarized in Table 1.

Table 1. Parameters Used in the Two Systems

Parameters ^a	Systems	
	Equilibrium ^b	Relaxation ^c
M	2.0×10^3	29164.4
ω	2.0×10^{-4}	9.0×10^{-3}
γ_{ext}	4.0×10^{-4}	0
Γ	1.0×10^{-4}	0.03675
g	20.6097	0.1
ΔG	-3.8×10^{-3}	0.09356
$k_B T$	9.5×10^{-4}	—
Time step (fs)	0.25	0.005
N_{traj}	500	5000

^aAll physical parameters are expressed in atomic units unless otherwise specified. ^bAdopted from ref 64. ^cApproximated from ref 66. See Support Information for details.

3.1. Equilibrium System Simulation. The 1D Newns–Anderson model (eq 31) is widely used to model equilibrium charge transfer between adsorbed molecules and metal surfaces.⁶³ Among the methods compared in previous studies,^{58,60,63,64} IESH stands out for its accuracy and adaptability to realistic systems. However, its computational cost becomes prohibitive when many bath orbitals are included.^{60,64} In this subsection, we show that our OSH algorithm achieves the same results as IESH but with significantly improved efficiency.

Figure 1 illustrates the impurity hole population ($1 - \langle c_a^\dagger c_a \rangle$) dynamics, where both OSH and IESH agree well with FCI-SH. We highlight that, despite being *completely* single-particle, OSH shows good agreement with FCI-SH in short-time dynamics, equilibrium population, and the overall population relaxation rate. Our results here numerically validate both the OSH and IESH ansätze, at least for a smaller system ($n_b = 10$). Applying FCI-SH to larger systems becomes impractical because the configuration space scales combinatorially with n_b (462 for $n_b = 10$). It is worth noting that a similar comparison between FCI-SH and IESH was conducted by Pradhan and Jain,⁵⁸ but their results differ from ours, showing considerable disagreement.

Figure 2 shows the convergence of hole population dynamics as we increase the number of orbitals, n_b . Notice that OSH agrees very well with IESH, and both results are

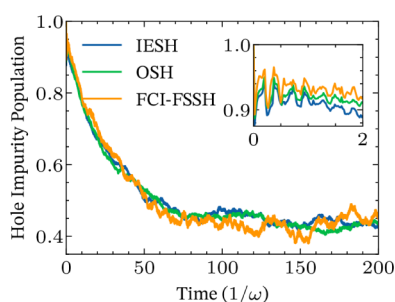


Figure 1. Impurity hole population dynamics as a function of time for OSH, IESH and FCI-FSSH. The inset shows the short-time behavior of the same dynamics. $n_b = 10$. $N_{\text{traj}} = 128$ for FCI-FSSH.

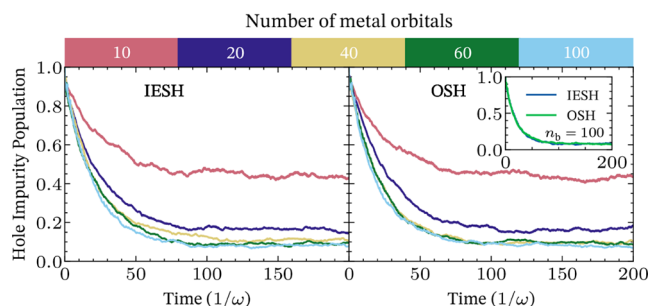


Figure 2. Convergence of the population dynamics over n_b . The left and right panels show results for IESH and OSH, respectively. Line colors correspond to the number of bath metal orbitals, as indicated in the top color palette. The inset in the right panel compares IESH and OSH when $n_b = 100$.

consistent with Figure 2a of ref 64. Here, OSH converges slightly faster with respect to n_b . Notably, the simulation cost of OSH is much lower than that of IESH, especially for large systems, where we observe a fourfold speedup when $n_b = 100$. The remarkable speedup of OSH arises from its simplicity: it requires only orbital density matrix elements σ_{ij} to calculate the hopping rate, whereas IESH must evaluate the determinant of overlap matrices for each possible hop. This is a well-known limitation of IESH, which necessitates optimized numerical algorithms for hopping probability⁶⁴ or upper-bound filtering⁶⁰ to mitigate the issue, but OSH inherently avoids this problem. A comparison of the efficiency between OSH and IESH is provided in the [Supporting Information](#).

3.2. Vibrational Relaxation Simulation. In this section, we showcase the performance of OSH in modeling the relaxation of a highly excited vibrational mode near a metal surface. Specifically, we investigate the relaxation of NO ($\nu = 16$) on a Au(111) surface, a system previously studied using IESH by various groups.^{27,60,67} For simplicity, our simulations focus solely on the NO stretching mode. For the vibrational frequency of the NO molecule, we refer to the computed value at the CASPT2/AVTZ level using the Beijing Density Functional (BDF) package⁶⁸ and the experimental value.⁶⁹ The double-well potential used in this study is parameterized based on ref 66 (see [Supporting Information](#) for details).

Similarly to Section 3.1, we start by comparing OSH and IESH with FCI-FSSH for a smaller n_b . Figure 3 shows consistent agreement among these methods, validating that OSH can predict the correct electron transfer dynamics even when the nuclear system is highly excited. Figure 3b depicts the kinetic energy relaxation dynamics of the NO molecule. In particular, all three methods predict identical short ($<20/\omega$)

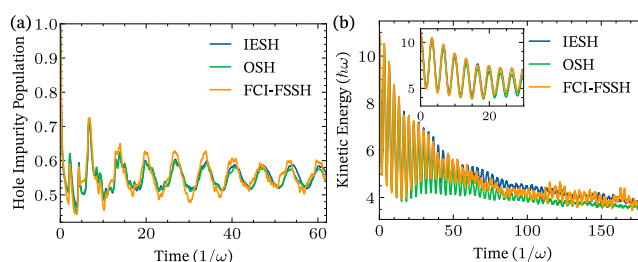


Figure 3. Comparison of OSH, IESH, and FCI-FSSH in modeling the relaxation of NO ($\nu = 16$) at the Au(111) surface. (a) Impurity hole population dynamics over time. (b) Kinetic energy evolution over time. $n_b = 10$. $N_{\text{traj}} = 512$ for FCI-FSSH.

and long ($>12/\omega$) time behavior of the kinetic energy. However, OSH predicts faster kinetic energy relaxation in the middle portion and relaxes to a slightly lower final kinetic energy than that of both IESH and FCI-FSSH.

Finally, we examine the convergence of NO's final vibrational distribution as n_b increases. Figure 4 shows that

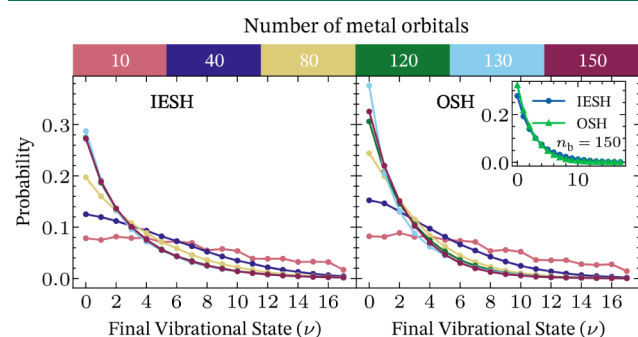


Figure 4. Convergence of the final vibrational state ν over n_b . The left and right panels show results for IESH and OSH, respectively. Line colors correspond to the number of bath metal orbitals, as indicated in the top color palette. The inset in the right panel compares IESH and OSH when $n_b = 150$.

the converged ν distribution peaks at $\nu = 0$ and decreases with increasing ν , a trend shared by OSH and IESH. However, OSH predicts higher probabilities for lower vibrational states, indicating greater relaxation to lower kinetic energy. Specifically, OSH converges to a final kinetic energy of $1.25 \hbar\omega$, compared to $2 \hbar\omega$ for IESH (see Figure 5). Additionally, IESH shows significantly higher kinetic energy than OSH during the transient period ($t < 50/\omega$). Notably, these simulations are highly expensive, requiring $n_b > 120$ and over 5000 trajectories to converge the ν distribution. Despite this, OSH can achieve a

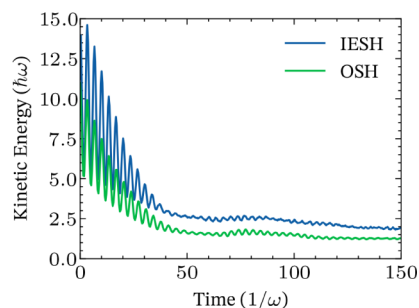


Figure 5. Kinetic energy of NO as a function of time for OSH and IESH. $n_b = 150$.

1.7× faster performance even when compared with a highly optimized IESH implementation⁶⁴ (see Supporting Information for details).

From our two test systems, we can address the questions posed at the beginning of this section. The simpler OSH approach yields results comparable to those of IESH. In fact, for a noninteracting system with fixed nuclear positions, the configuration interaction with single substitutions (CIS), whose wave function is constructed from a single determinant, produces the same energy levels as the full configuration interaction (FCI) method. Moreover, the forces and derivative couplings obtained from the CIS method are identical to those from the FCI method. Our results demonstrate that many-body effects are properly accounted for in nonadiabatic dynamics.

In addition, one advantage of the OSH method is its ability to handle mixed states rather than just pure states. This capability allows for the integration of a thermostat into OSH more easily than in IESH. Literature has shown that IESH fails to achieve detailed balance in the long-time limit.⁶⁴ With the addition of a thermostat to IESH, the dynamics may become inaccurate. In contrast, we expect that OSH can provide both the correct dynamics and detailed balance when a thermostat is incorporated. This work is ongoing.

4. CONCLUSIONS

We have introduced orbital surface hopping (OSH), a novel and efficient algorithm for modeling noninteracting multi-electron systems. This algorithm is motivated by the orbital quantum-classical Liouville equation (o-QCLE), which is exactly derived as a quantum-classical approximation of the Liouville equation for the reduced many-body density matrix. OSH is applied to study electron and energy transfer dynamics in molecule–metal surfaces, demonstrating results that are identical or comparable to those of the independent electron surface hopping (IESH) algorithm but at significantly lower computational cost. Two scenarios are examined: for electron transfer at thermal equilibrium, OSH and IESH produced nearly identical results. For vibrational relaxation of highly excited molecules, OSH and IESH yielded similar vibrational distributions, though OSH predicted greater energy transfer from molecular vibrations to the metal surface. Notably, for large systems with over 100 orbitals, OSH achieves an approximately 2× speedup compared to an efficient implementation of IESH.

Since the OSH method is based on the mixed quantum-classical Liouville equation in the orbital basis, the o-QCLE is restricted to noninteracting electrons. The OSH method approximates the o-QCLE in a fashion similar to FSSH; thus, it is also limited to the case of noninteracting electrons. In contrast to methods such as HEOM or BCME, where the metal is treated as a continuum, OSH explicitly treats the metal, providing greater flexibility for different band structures. Furthermore, as highlighted in the previous discussion, it has been shown in the literature that IESH does not yield detailed balance in the long-time limit, even when additional discrete levels are added.⁶⁴ Since numerically exact methods such as HEOM treat the electronic continuum as a bath, a direct comparison of HEOM with OSH (or IESH) is not strictly justified. One way to achieve the continuum limit for OSH is by adding a thermostat. In the future, we plan to introduce a thermostat in the OSH method to achieve the continuum limit. This project is in progress.

APPENDIX A

A. Derivation of the orbital Liouville-von Neumann equation (eq 4)

Apply $\hat{d}_i^\dagger \hat{d}_j$ from the right to both sides of eq 3, and then take the trace over the electronic degrees of freedom,

$$\frac{\partial \hat{\sigma}_{ji}}{\partial t} = -\frac{i}{\hbar} \left\{ \text{Tr}_e(\hat{H}_{\text{total}} \hat{\rho} \hat{d}_i^\dagger \hat{d}_j) - \text{Tr}_e(\hat{\rho} \hat{H}_{\text{total}} \hat{d}_i^\dagger \hat{d}_j) \right\} \quad (36)$$

Realize that \hat{T}_n and $U(\hat{\mathbf{R}})$ commute with the creation and annihilation operators and can be moved out of the trace; hence

$$\frac{\partial \hat{\sigma}_{ji}}{\partial t} = -\frac{i}{\hbar} \sum_{kl} \left\{ h_{kl}(\hat{\mathbf{R}}) \text{Tr}_e(\hat{d}_k^\dagger \hat{d}_l \hat{\rho} \hat{d}_i^\dagger \hat{d}_j) - \text{Tr}_e(\hat{\rho} \hat{d}_k^\dagger \hat{d}_l \hat{d}_i^\dagger \hat{d}_j) h_{kl}(\hat{\mathbf{R}}) \right\} - \frac{i}{\hbar} [\hat{T}_n, \hat{\sigma}_{ij}] - \frac{i}{\hbar} [U(\hat{\mathbf{R}}), \hat{\sigma}_{ij}] \quad (37)$$

Then, apply the anti-commutation relation $\{\hat{d}_i^\dagger \hat{d}_j\} = \delta_{ij}$ and the cyclic properties of the trace, we have

$$\begin{aligned} \text{Tr}_e(\hat{d}_k^\dagger \hat{d}_l \hat{\rho} \hat{d}_i^\dagger \hat{d}_j) &= \hat{\sigma}_{il} \delta_{jk} - \text{Tr}_e(\hat{d}_i^\dagger \hat{d}_k \hat{\rho} \hat{d}_l \hat{d}_j) \\ \text{Tr}_e(\hat{\rho} \hat{d}_k^\dagger \hat{d}_l \hat{d}_i^\dagger \hat{d}_j) &= \hat{\sigma}_{jk} \delta_{il} - \text{Tr}_e(\hat{\rho} \hat{d}_k^\dagger \hat{d}_i \hat{d}_l \hat{d}_j) \end{aligned} \quad (38)$$

The second terms of the above two equations cancel each other out since $\{\hat{d}_i^\dagger \hat{d}_j\} = \{\hat{d}_i^\dagger \hat{d}_j^\dagger\} = 0$. Meanwhile, for the first term, swapping the dummy index $k \leftrightarrow l$ in the second line leads to

$$\begin{aligned} &\sum_{kl} h_{kl}(\hat{\mathbf{R}}) [\text{Tr}_e(\hat{d}_k^\dagger \hat{d}_l \hat{\rho} \hat{d}_i^\dagger \hat{d}_j) - \text{Tr}_e(\hat{\rho} \hat{d}_k^\dagger \hat{d}_l \hat{d}_i^\dagger \hat{d}_j)] \\ &= \sum_{kl} [h_{kl}(\hat{\mathbf{R}}) \hat{\sigma}_{il} \delta_{jk} - h_{lk}(\hat{\mathbf{R}}) \hat{\sigma}_{jl} \delta_{ik}] \\ &= \sum_l [h_{ji}(\hat{\mathbf{R}}) \hat{\sigma}_{il} - \hat{\sigma}_{jl} h_{li}(\hat{\mathbf{R}})] \end{aligned} \quad (39)$$

Hence, we have proved eq 4, i.e., the LvN for single-body orbitals.

B. Derivation of the First Order Derivative Coupling (DC) of Different States

Consider the DC between two adiabatic states $j(|j\rangle = |j_1, j_2, \dots, j_{N_e}\rangle)$ and $k(|k\rangle = |k_1, k_2, \dots, k_{N_e}\rangle)$:

$$\left\langle j \left| \frac{\partial \mathbf{k}}{\partial \mathbf{R}} \right. \right\rangle = \frac{\langle j | \frac{\partial \hat{H}_{el}}{\partial \mathbf{R}} | k \rangle}{E_k - E_j} \quad (40)$$

Use the unit projector $\mathbf{1} = \sum_m |m\rangle \langle m| = \sum_n |n\rangle \langle n|$

$$\begin{aligned}
 & \frac{\langle j | \frac{\partial \hat{H}_i}{\partial R} | k \rangle}{E_k - E_j} \\
 &= \frac{\sum_{mm}^{N_{\text{orb}}} \langle j | m \rangle \langle m | \frac{\partial \hat{H}_i}{\partial R} | n \rangle \langle n | k \rangle}{E_k - E_j} \\
 &= \frac{\sum_{mm}^{N_{\text{orb}}} \langle j | m \rangle d_{mn} (\epsilon_n - \epsilon_m) \langle n | k \rangle}{\sum_{kj}^{N_{\text{el}}} (\epsilon_k - \epsilon_j)} \\
 &= \frac{\sum_{mm}^{N_{\text{orb}}} \langle j | d_{mn} (\epsilon_n - \epsilon_m) b_n^\dagger b_n | k \rangle}{\sum_{kj}^{N_{\text{el}}} (\epsilon_k - \epsilon_j)} \\
 &= \frac{\sum_{mm}^{N_{\text{orb}}} d_{mn} (\epsilon_n - \epsilon_m) \langle j | b_n^\dagger b_n | k \rangle}{\sum_{kj}^{N_{\text{el}}} (\epsilon_k - \epsilon_j)} \\
 &= d_{kj}
 \end{aligned}$$

The last step uses the orthonormality property of the adiabatic orbital. The subscript of i stands for the i^{th} electron, which is used to accomplish the antisymmetry of electrons.

C. Comparison of the Hopping Probabilities Between the IESH and OSH Methods

In the IESH, the density matrix elements are calculated as

$$\rho_{IJ} \equiv \langle I | \Psi \rangle \langle \Psi | J \rangle \quad (41)$$

Similar to fewest switches surface hopping (FSSH), the hopping probabilities from an active state I to state J is given by

$$\frac{-2\text{Re}[A_{IJ}(v \cdot D)_{IJ}]}{A_{II}} = \frac{-2\text{Re}[\rho_{IJ}(v \cdot D)_{IJ}]}{\rho_{II}} \quad (42)$$

For an electronically non-interacting system, only single electron hop needs to be considered in a hopping event, as proven in Appendix B.

$$\frac{-2\text{Re}[\rho_{IJ}(v \cdot D)_{IJ}]}{\rho_{II}} = \frac{-2\text{Re}[\rho_{IJ}(v \cdot d)_{ij}]}{\rho_{II}} \quad (43)$$

In OSH, the hopping probabilities of one electron hops from orbital i to orbital j can be derived from the o-QCLE (eq 11),

$$g_{ij} = \frac{-2\text{Re}[\sigma_{ji}(v \cdot d)_{ij}]}{\sigma_{ii}} \quad (44)$$

With the definition of the orbital density matrix, it can be represented as

$$\begin{aligned}
 \hat{\sigma}_{ij} &= \text{Tr}_e(\hat{\rho} d_j^\dagger d_i) \\
 &= \sum_I \langle I | (|\Psi\rangle \langle \Psi| d_j^\dagger d_i) | I \rangle \\
 &= \sum_I \rho_{IJ}
 \end{aligned} \quad (45)$$

Note that in this equation, the trace over electronic states has been replaced by a summation over all electronic states. In the diagonal case, the orbital density matrix element is given by $\sigma_{ii} = \sum_I \rho_{II}$. Substituting these two equations into the expression for the hopping probabilities, we obtain

$$\begin{aligned}
 & -2 \frac{\sum_I \text{Re}[\rho_{IJ}(v \cdot d)_{ij}]}{\sum_I \rho_{II}} \\
 &= -2 \frac{\text{Re}[\rho_{IJ}(v \cdot d)_{ij}] + \sum_{K \neq I} \text{Re}[\rho_{JK}(v \cdot d)_{ij}]}{\rho_{II} + \sum_{K \neq I} \rho_{KK}} \quad (46)
 \end{aligned}$$

From this equation, we can see that while the hopping probabilities in IESH and OSH share similarities, they are not identical. Specifically, IESH considers only the hopping of the active state to its single excitations, whereas OSH, derived from the o-QCLE framework, accounts for single excitations from all possible states that include the active orbital. As a result, the hopping probabilities in OSH retain characteristics of a mixed-state approach, reflecting the density matrix nature of this method.

■ ASSOCIATED CONTENT

Supporting Information

The Supporting Information is available free of charge at <https://pubs.acs.org/doi/10.1021/acs.jctc.4c01769>.

Potential energy surface for NO-Au(111) system and simulation cost comparison of OSH, IESH, FCI-SH methods (PDF)

■ AUTHOR INFORMATION

Corresponding Author

Wenjie Dou – Department of Chemistry, School of Science and Research Center for Industries of the Future and Key Laboratory for Quantum Materials of Zhejiang Province, Department of Physics, School of Science and Research Center for Industries of the Future, Westlake University, Hangzhou, Zhejiang 310024, China; Institute of Natural Sciences, Westlake Institute for Advanced Study, Hangzhou, Zhejiang 310024, China; orcid.org/0000-0001-5410-6183; Email: douwenjie@westlake.edu.cn

Authors

Yong-Tao Ma – Department of Chemistry, School of Science and Research Center for Industries of the Future, Westlake University, Hangzhou, Zhejiang 310024, China; orcid.org/0009-0009-6524-8801

Rui-Hao Bi – Department of Chemistry, School of Science and Research Center for Industries of the Future, Westlake University, Hangzhou, Zhejiang 310024, China; orcid.org/0000-0001-7135-5368

Complete contact information is available at: <https://pubs.acs.org/10.1021/acs.jctc.4c01769>

Author Contributions

^{||}Y.-T.M. and R.-H.B. contributed equally to this work

Notes

The authors declare no competing financial interest.

■ ACKNOWLEDGMENTS

W.D. acknowledges funding from the National Natural Science Foundation of China (No. 22361142829) and the Zhejiang Provincial Natural Science Foundation (No. XHD24B0301). Y.-T. Ma expressed gratitude for support from the Shandong Provincial Natural Science Foundation (Grant No. ZR2021MB081), gratefully acknowledged HZWTECH for providing computation facilities, and thanked Chongxiao Zhao

and Yunhao Liu for their helpful discussion on second quantization theory. The authors also extended their thanks to the Westlake University Supercomputer Center for providing facility support and technical assistance.

REFERENCES

- (1) Wodtke, A.M.; Tully, J.C.; Auerbach, D.J. Electronically non-adiabatic interactions of molecules at metal surfaces: Can we trust the Born-Oppenheimer approximation for surface chemistry? *Int. Rev. Phys. Chem.* **2004**, *23*, 513–539.
- (2) White, J. D.; Chen, J.; Matsiev, D.; Auerbach, D. J.; Wodtke, A. M. Conversion of large-amplitude vibration to electron excitation at a metal surface. *Nature* **2005**, *433*, 503–505.
- (3) Huang, Y.; Rettner, C. T.; Auerbach, D. J.; Wodtke, A. M. Vibrational Promotion of Electron Transfer. *Science* **2000**, *290*, 111–114.
- (4) Huang, Y.; Wodtke, A. M.; Hou, H.; Rettner, C. T.; Auerbach, D. J. Observation of Vibrational Excitation and Deexcitation for NO ($\nu = 2$) Scattering from Au(111): Evidence for Electron-Hole-Pair Mediated Energy Transfer. *Phys. Rev. Lett.* **2000**, *84*, 2985–2988.
- (5) Tully, J. C. Chemical Dynamics at Metal Surfaces. *Annu. Rev. Phys. Chem.* **2000**, *51*, 153–178.
- (6) Buneremann, O.; Jiang, H.; Dorenkamp, Y.; Kandratsenka, A.; Janke, S. M.; Auerbach, D. J.; Wodtke, A. M. Electron-hole pair excitation determines the mechanism of hydrogen atom adsorption. *Science* **2015**, *350*, 1346–1349.
- (7) Krüger, B. C.; Meyer, S.; Kandratsenka, A.; Wodtke, A. M.; Schäfer, T. Vibrational Inelasticity of Highly Vibrationally Excited NO on Ag(111). *J. Phys. Chem. Lett.* **2016**, *7*, 441–446.
- (8) Geweke, J.; Wodtke, A. M. Vibrationally inelastic scattering of HCl from Ag(111). *J. Chem. Phys.* **2020**, *153* (16), 164703.
- (9) Lam, Y.-C.; Soudackov, A. V.; Hammes-Schiffer, S. Theory of Electrochemical Proton-Coupled Electron Transfer in Diabatic Vibronic Representation: Application to Proton Discharge on Metal Electrodes in Alkaline Solution. *J. Phys. Chem. C* **2020**, *124*, 27309–27322.
- (10) Lee, S. W.; Jeon, B.; Lee, H.; Park, J. Y. Hot Electron Phenomena at Solid–Liquid Interfaces. *J. Phys. Chem. Lett.* **2022**, *13*, 9435–9448.
- (11) Luo, X.; Jiang, B.; Juaristi, J. I.; Alducin, M.; Guo, H. Electron-hole pair effects in methane dissociative chemisorption on Ni(111). *J. Chem. Phys.* **2016**, *145* (4), 044704.
- (12) Dorenkamp, Y.; Jiang, H.; Köckert, H.; Hertl, N.; Kammler, M.; Janke, S. M.; Kandratsenka, A.; Wodtke, A. M.; Bünermann, O. Hydrogen collisions with transition metal surfaces: Universal electronically nonadiabatic adsorption. *J. Chem. Phys.* **2018**, *148*, 034706.
- (13) Ke, Y.; Erpenbeck, A.; Peskin, U.; Thoss, M. Unraveling current-induced dissociation mechanisms in single-molecule junctions. *J. Chem. Phys.* **2021**, *154* (23), 234702.
- (14) Teh, H.-H.; Dou, W.; Subotnik, J. E. Spin polarization through a molecular junction based on nuclear Berry curvature effects. *Phys. Rev. B* **2022**, *106*, 184302.
- (15) Beck, M.; Jäckle, A.; Worth, G.; Meyer, H.-D. The multiconfiguration time-dependent Hartree (MCTDH) method: A highly efficient algorithm for propagating wavepackets. *Phys. Rep.* **2000**, *324*, 1–105.
- (16) Xu, M.; Liu, Y.; Song, K.; Shi, Q. A non-perturbative approach to simulate heterogeneous electron transfer dynamics: Effective mode treatment of the continuum electronic states. *J. Chem. Phys.* **2019**, *150* (4), 044109.
- (17) Dou, W.; Miao, G.; Subotnik, J. E. Born-Oppenheimer Dynamics, Electronic Friction, and the Inclusion of Electron-Electron Interactions. *Phys. Rev. Lett.* **2017**, *119*, 046001.
- (18) Smith, B. B.; Hynes, J. T. Electronic friction and electron transfer rates at metallic electrodes. *J. Chem. Phys.* **1993**, *99*, 6517–6530.
- (19) d’Agliano, E. G.; Kumar, P.; Schaich, W.; Suhl, H. Brownian motion model of the interactions between chemical species and metallic electrons: Bootstrap derivation and parameter evaluation. *Phys. Rev. B* **1975**, *11*, 2122–2143.
- (20) Brandbyge, M.; Hedegård, P.; Heinz, T. F.; Misewich, J. A.; News, D. M. Electronically driven adsorbate excitation mechanism in femtosecond-pulse laser desorption. *Phys. Rev. B* **1995**, *52*, 6042–6056.
- (21) Head-Gordon, M.; Tully, J. C. Molecular dynamics with electronic frictions. *J. Chem. Phys.* **1995**, *103*, 10137–10145.
- (22) Dou, W.; Nitzan, A.; Subotnik, J. E. Frictional effects near a metal surface. *J. Chem. Phys.* **2015**, *143* (5), 054103.
- (23) Dou, W.; Subotnik, J. E. A many-body states picture of electronic friction: The case of multiple orbitals and multiple electronic states. *J. Chem. Phys.* **2016**, *145* (5), 054102.
- (24) Bode, N.; Kusminskiy, S. V.; Egger, R.; von Oppen, F. Scattering Theory of Current-Induced Forces in Mesoscopic Systems. *Phys. Rev. Lett.* **2011**, *107*, 036804.
- (25) Lü, J.-T.; Brandbyge, M.; Hedegård, P.; Todorov, T. N.; Dundas, D. Current-induced atomic dynamics, instabilities, and Raman signals: Quasiclassical Langevin equation approach. *Phys. Rev. B* **2012**, *85*, 245444.
- (26) Persson, B.; Persson, M. Vibrational lifetime for CO adsorbed on Cu(100). *Solid State Commun.* **1980**, *36*, 175–179.
- (27) Shenvi, N.; Roy, S.; Tully, J. C. Nonadiabatic dynamics at metal surfaces: Independent-electron surface hopping. *J. Chem. Phys.* **2009**, *130* (17), 174107.
- (28) Shenvi, N.; Tully, J. C. Nonadiabatic dynamics at metal surfaces: Independent electron surface hopping with phonon and electron thermostats. *Faraday Discuss* **2012**, *157*, 325–335.
- (29) Malpathak, S.; Ananth, N. A Linearized Semiclassical Dynamics Study of the Multiquantum Vibrational Relaxation of NO Scattering from a Au(111) Surface. *J. Phys. Chem. Lett.* **2024**, *15*, 794–801. PMID: 38232133.
- (30) Dou, W.; Nitzan, A.; Subotnik, J. E. Surface hopping with a manifold of electronic states. II. Application to the many-body Anderson-Holstein model. *J. Chem. Phys.* **2015**, *142* (8), 084110.
- (31) Dou, W.; Nitzan, A.; Subotnik, J. E. Surface hopping with a manifold of electronic states. III. Transients, broadening, and the Marcus picture. *J. Chem. Phys.* **2015**, *142* (23), 234106.
- (32) Dou, W.; Subotnik, J. E. Perspective: How to understand electronic friction. *J. Chem. Phys.* **2018**, *148* (23), 230901.
- (33) Wang, Y.; Jia, Y. A path integral approach to electronic friction of a nanometer-sized tip scanning a metal surface. *Commun. Theor. Phys.* **2021**, *73*, 045701.
- (34) Martinazzo, R.; Burghardt, I. Quantum Dynamics with Electronic Friction. *Phys. Rev. Lett.* **2022**, *128*, 206002.
- (35) Martinazzo, R.; Burghardt, I. Quantum theory of electronic friction. *Phys. Rev. A* **2022**, *105*, 052215.
- (36) Spiering, P.; Meyer, J. Testing Electronic Friction Models: Vibrational De-excitation in Scattering of H₂ and D₂ from Cu(111). *J. Phys. Chem. Lett.* **2018**, *9*, 1803–1808. PMID: 29528648.
- (37) Zhang, Y.; Maurer, R. J.; Jiang, B. Symmetry-Adapted High Dimensional Neural Network Representation of Electronic Friction Tensor of Adsorbates on Metals. *J. Phys. Chem. C* **2020**, *124*, 186–195.
- (38) Zhou, X.; Meng, G.; Guo, H.; Jiang, B. First-Principles Insights into Adiabatic and Nonadiabatic Vibrational Energy-Transfer Dynamics during Molecular Scattering from Metal Surfaces: The Importance of Surface Reactivity. *J. Phys. Chem. Lett.* **2022**, *13*, 3450–3461. PMID: 35412832.
- (39) Gardner, J.; Habershon, S.; Maurer, R. J. Assessing Mixed Quantum-Classical Molecular Dynamics Methods for Nonadiabatic Dynamics of Molecules on Metal Surfaces. *J. Phys. Chem. C* **2023**, *127*, 15257–15270.
- (40) Bui, A. T.; Thiemann, F. L.; Michaelides, A.; Cox, S. J. Classical Quantum Friction at Water-Carbon Interfaces. *Nano Lett.* **2023**, *23*, 580–587. PMID: 36626824.

- (41) Wang, Y.; Dou, W. Nonadiabatic dynamics near metal surfaces under Floquet engineering: Floquet electronic friction vs Floquet surface hopping. *J. Chem. Phys.* **2023**, *159* (9), 094103.
- (42) Mosallanejad, V.; Chen, J.; Dou, W. Floquet-driven frictional effects. *Phys. Rev. B* **2023**, *107*, 184314.
- (43) Chen, J.; Liu, W.; Mosallanejad, V.; Dou, W. Floquet Nonadiabatic Nuclear Dynamics with Photoinduced Lorentz-like Force in Quantum Transport. *J. Phys. Chem. C* **2024**, *128*, 11219–11228.
- (44) Craig, C. F.; Duncan, W. R.; Prezhdo, O. V. Trajectory Surface Hopping in the Time-Dependent Kohn-Sham Approach for Electron-Nuclear Dynamics. *Phys. Rev. Lett.* **2005**, *95*, 163001.
- (45) Habenicht, B. F.; Craig, C. F.; Prezhdo, O. V. Time-Domain Ab Initio Simulation of Electron and Hole Relaxation Dynamics in a Single-Wall Semiconducting Carbon Nanotube. *Phys. Rev. Lett.* **2006**, *96*, 187401.
- (46) Akimov, A. V.; Prezhdo, O. V. The PYXAID Program for Non-Adiabatic Molecular Dynamics in Condensed Matter Systems. *J. Chem. Theory Comput.* **2013**, *9*, 4959–4972. PMID: 26583414.
- (47) Shenvi, N.; Roy, S.; Tully, J. C. Dynamical Steering and Electronic Excitation in NO Scattering from a Gold Surface. *Science* **2009**, *326*, 829–832.
- (48) Roy, S.; Shenvi, N.; Tully, J. C. Dynamics of Open-Shell Species at Metal Surfaces. *J. Phys. Chem. C* **2009**, *113*, 16311–16320.
- (49) Kapral, R.; Ciccotti, G. Mixed quantum-classical dynamics. *J. Chem. Phys.* **1999**, *110*, 8919–8929.
- (50) Subotnik, J. E. Augmented Ehrenfest dynamics yields a rate for surface hopping. *J. Chem. Phys.* **2010**, *132*, 134112.
- (51) Subotnik, J. E.; Ouyang, W.; Landry, B. R. Can we derive Tully's surface-hopping algorithm from the semiclassical quantum Liouville equation? Almost, but only with decoherence. *J. Chem. Phys.* **2013**, *139*, 214107.
- (52) Mannouch, J. R.; Richardson, J. O. A mapping approach to surface hopping. *J. Chem. Phys.* **2023**, *158*, 104111.
- (53) Nielsen, S.; Kapral, R.; Ciccotti, G. Mixed quantum-classical surface hopping dynamics. *J. Chem. Phys.* **2000**, *112*, 6543–6553.
- (54) Kapral, R. Surface hopping from the perspective of quantum-classical Liouville dynamics. *Chem. Phys.* **2016**, *481*, 77–83.
- (55) Tully, J. C. Molecular dynamics with electronic transitions. *J. Chem. Phys.* **1990**, *93*, 1061–1071.
- (56) Hammes-Schiffer, S.; Tully, J. C. Proton transfer in solution: Molecular dynamics with quantum transitions. *J. Chem. Phys.* **1994**, *101*, 4657–4667.
- (57) Landry, B. R.; Falk, M. J.; Subotnik, J. E. Communication: The correct interpretation of surface hopping trajectories: How to calculate electronic properties. *J. Chem. Phys.* **2013**, *139*, 211101.
- (58) Pradhan, C. S.; Jain, A. Detailed Balance and Independent Electron Surface-Hopping Method: The Importance of Decoherence and Correct Calculation of Diabatic Populations. *J. Chem. Theory Comput.* **2022**, *18*, 4615–4626. PMID: 35880817.
- (59) Poshusta, R. D. Algebrants in many electron quantum mechanics. II. New computational algorithms. *Int. J. Quantum Chem.* **1991**, *40*, 225–234.
- (60) Gardner, J.; Corken, D.; Janke, S. M.; Habershon, S.; Maurer, R. J. Efficient implementation and performance analysis of the independent electron surface hopping method for dynamics at metal surfaces. *J. Chem. Phys.* **2023**, *158*, 064101.
- (61) Szabó, A.; Ostlund, N. S. *Modern quantum chemistry: Introduction to advanced electronic structure theory*; Dover publications: Mineola, N.Y., 1996.
- (62) Subotnik, J. E.; Ouyang, W.; Landry, B. R. Can we derive Tully's surface-hopping algorithm from the semiclassical quantum Liouville equation? Almost, but only with decoherence. *J. Chem. Phys.* **2013**, *139*, 214107.
- (63) Ouyang, W.; Dou, W.; Jain, A.; Subotnik, J. E. Dynamics of Barrier Crossings for the Generalized Anderson-Holstein Model: Beyond Electronic Friction and Conventional Surface Hopping. *J. Chem. Theory Comput.* **2016**, *12*, 4178–4183. PMID: 27564005.
- (64) Miao, G.; Ouyang, W.; Subotnik, J. A comparison of surface hopping approaches for capturing metal-molecule electron transfer: A broadened classical master equation versus independent electron surface hopping. *J. Chem. Phys.* **2018**, *150*, 041711.
- (65) Sun, L.; Hase, W. L. Comparisons of classical and Wigner sampling of transition state energy levels for quasiclassical trajectory chemical dynamics simulations. *J. Chem. Phys.* **2010**, *133*, 044313.
- (66) Meng, G.; Jiang, B. A pragmatic protocol for determining charge transfer states of molecules at metal surfaces by constrained density functional theory. *J. Chem. Phys.* **2022**, *157*, 214103.
- (67) Meng, G.; Gardner, J.; Hertl, N.; Dou, W.; Maurer, R. J.; Jiang, B. First-Principles Nonadiabatic Dynamics of Molecules at Metal Surfaces with Vibrationally Coupled Electron Transfer. *Phys. Rev. Lett.* **2024**, *133*, 036203.
- (68) Zhang, Y.; Suo, B.; Wang, Z.; Zhang, N.; Li, Z.; Lei, Y.; Zou, W.; Gao, J.; Peng, D.; Pu, Z.; Xiao, Y.; Sun, Q.; Wang, F.; Ma, Y.; Wang, X.; Guo, Y.; Liu, W. BDF: A relativistic electronic structure program package. *J. Chem. Phys.* **2020**, *152* (6), 064113.
- (69) Reddy, R.R.; Nazeer Ahammed, Y.; Baba Basha, D.; Narasimhulu, K.; Siva Sankar Reddy, L.; Rama Gopal, K. Spectroscopic studies of atmospheric interest on NO and NO+. *J. Quant. Spectrosc. Radiat. Transfer* **2006**, *97*, 344.

NOTE ADDED AFTER ASAP PUBLICATION

Due to a production error, the version of this article that was published ASAP March 21, 2025, contained errors in two equations: First, an error in the unlabeled display equation before eq 41; second, an error in eq 46. These were corrected and the paper reposted March 31, 2025.